EGRET Observations of Diffuse Gamma-Ray Emission in Taurus and Perseus

S. W. Digel (USRA/NASA GSFC) & I. A. Grenier (Université Paris 7 and Service d'Astrophysique, CE Saclay)

Abstract

We present an analysis of the interstellar gamma-ray emission observed toward the extensive molecular cloud complexes in Taurus and Perseus by the Energetic Gamma-Ray Experiment Telescope (EGRET). The region's large size (more than 300 square degrees) and location below the plane in the anticenter are advantageous for straightforward interpretation of the interstellar emission. The complex of clouds in Taurus has a distance of ~140 pc and is near the center of the Gould Belt. The complex in Perseus, adjacent to Taurus on the sky, is near the rim of the Belt at a distance of ~300 pc. The findings for the cosmic-ray density and the molecular mass-calibrating ratio $N(H_2)/W_{CO}$ in Taurus and Perseus are compared with results for other nearby cloud complexes resolved by EGRET. The local clouds that now have been studied in gamma rays can be used to trace the distribution of high-energy cosmic rays within 1 kpc of the sun.

1. Introduction

The gamma-ray emissions from the interactions of high-energy cosmic rays with interstellar nucleons have long been used to study the densities of cosmic-rays and the column densities of molecular gas in the Milky Way (e.g. Lebrun et al. 1983). The low instrumental background, good point-spread function, and long life of the Energetic Gamma-Ray Experiment Telescope (EGRET) made possible great advances in the study of interstellar emission. In particular, EGRET spatially resolved a number of nearby (distances up to hundreds of pc) interstellar cloud complexes. Local cloud complexes are of interest for study in diffuse gamma rays because they permit the most sensitive searches for variations of cosmic-ray density and molecular mass calibration within clouds. They are also of interest because the cosmic-ray density in the solar vicinity can be 'mapped' by studies of the local cloud complexes.

Several local cloud complexes already have been investigated in detail with EGRET data, and we report here a study of the diffuse emission in Taurus and Perseus (l = 150° to 185°, b = -30° to -5°), two of the last large local complexes to be analyzed. The Taurus-Perseus region poses some unique challenges to the interpretation of the diffuse gamma-ray emission owing to its closeness to the Galactic anticenter and to the bright emission of the Crab pulsar. We describe our findings in the context of other studies of other local clouds with EGRET.

2. Data

2.1. Gamma-Ray

We use composite photon counts and exposure maps constructed from all data from Phases 1–5. For viewing periods when EGRET was operated in full field-of-view mode, only directions within 30° of the instrument axis were included in the composite maps. The point-spread function and energy resolution rapidly degrade at larger inclination angles. Owing to the corresponding decrease in effective area at large angles, little data are lost, and by cutting the data at 30° the simplifying assumption can be made that a single set of point-spread functions applies to the composite dataset. The standard sensitivity corrections for the ageing of the spark chamber gas were used.

The exposure of EGRET for the representative energy range 100–10,000 MeV is shown in **Figure 1**. The large gradient is due to the many observations of the Crab.

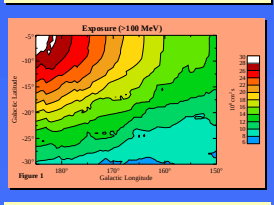

Figure 1

2.2. CO & H I

The intensity of the 2.6-mm J = 1–0 line of CO is commonly used as a tracer for the column density of H_2, which although the dominant constituent of the dense interstellar medium is rarely directly observed at interstellar conditions. CO is the second most abundant interstellar molecule and empirically the integrated intensity W_{CO} of the 2.6-mm line is proportional to $N(H_2)$ (e.g., Dickman 1978). The ratio $N(H_2)/W_{CO}$ is conventionally denoted X. Diffuse gamma-ray emission has long been recognized as an indirect tracer of interstellar gas useful for calibrating X.

We use the new composite-CO survey of Dame, Hartmann, & Thaddeus (2001) for the analysis presented here (**Fig. 2a**). The molecular clouds in Taurus (~140 pc distant) are superposed on the ~300 pc distant clouds in Perseus in this view. The data were rebinned to the 0.5° grid of the gamma-ray maps.

We derive $N(H\,I)$ from the 21-cm line Leiden-Dwingeloo survey (Hartmann & Burton 1997, **Fig. 2b**). A spin temperature of 125 K was assumed for the minor correction for optical depth.

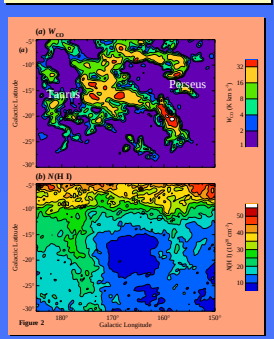

Figure 2

3. Analysis

Because high-energy cosmic rays uniformly penetrate interstellar gas, and because the interstellar medium is optically thin to gamma rays, in principle the diffuse gamma-ray intensity can be well modelled as a linear combination of the $N(H\,I)$ and $I(CO)$ maps plus the isotropic extragalactic background. However, the closeness of the Taurus/Perseus region to the anticenter complicates the analysis. In other directions, differential rotation of the Galaxy permits components of the gas at different distances (where the cosmic-ray density may be different) to be distinguished by their line-of-sight velocities. In the anticenter, however, the gradient of velocity with distance vanishes. This is particularly important for H I, which can be detected throughout the Galaxy. Lines of sight close to the plane include gas at great distances in the outer Galaxy for which the cosmic-ray density is much less than it is locally.

A variety of approaches for accommodating the absence of distance discriminators in the H I spectra were investigated. A simple approach that led to the quantitatively best fitting models was to assume that the gamma-ray emissivity of the atomic gas is constant (independent of direction) for b < -15° but varies linearly with latitude for b > -15°. The constant and slope are free parameters in the model.

For the present analysis, we exclude the region within 10° of the Crab pulsar. The pulsar is such a bright gamma-ray source that its emission must otherwise be carefully modelled in the tails of the point-spread function.

As for other studies of diffuse gamma-ray emission (e.g., Digel et al. 200 I), a search was made for gamma-ray point sources in the region under study by evaluating the likelihood test statistic systematically for a grid of positions spanning the region.

The final model for the gamma-ray intensity in Taurus/Perseus may be written as

$$I(l,b) = \left[A + B\Theta\left(b+15^\circ\right)\times\left(b+15^\circ\right)\right]N(\mathrm{H\,I}) + C W_{CO} + D + \sum_k E_k \delta\left(l-l_k, b-b_k\right) \quad (1)$$

for any given energy range. Θ is the Heaviside step function; $\Theta(x) = 0$ for $x < 0$ and $\Theta(x) = 1$ for $x \geq 0$. A (units photons s^{-1}sr^{-1}) is the gamma-ray emissivity for (b < -45°), and B is the slope (photons s^{-1}sr^{-1}deg^{-1}) for b > -15°. $C = 2\Delta X$, where $X = N(H_2)/W_{CO}$ is the effective conversion factor by CO ((atoms cm^{-2})/(K km s^{-1})), and D is the intensity of the isotropic background emission (photons s^{-1}cm^{-2}sr^{-1}). The E_k are the fluxes of the point sources (photons cm^{-2}s^{-1}) included in the model.

Taking into account the distribution of exposure ε and the effective (energy and effective-area weighted) point-spread function PSF, the corresponding model distribution of photons is

$$\sigma(l,b) = \left[A + B\Theta\left(b+15^\circ\right)\times\left(b+15^\circ\right)\right]N(\mathrm{H\,I}) + C W_{CO_{ex}} + D\varepsilon_{ex} + \sum_k E_k PSF\left(l-l_k, b-b_k\right)\varepsilon\left(l_k, b_k\right) \quad (2)$$

where the subscript 'ex' indicates multiplication with the exposure map and convolution with the effective point-spread function $PSF(x,y)$. ε_x is the exposure map itself convolved with the effective point-spread function.

As for other studies of EGRET data, the model was fit to the observations using the maximum likelihood method (Mattox et al. 1996). The observed numbers of photons in each 0.5×0.5 deg^2 pixel in the region of interest were compared with the predictions of the model (Eq. 2) and the parameters of the model were adjusted to maximize the overall Poisson probability.

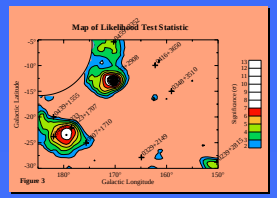

Figure 3

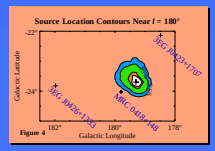

Figure 4

Table 1 – Point Sources in the Taurus/Perseus Model

Name	l	b	Flux (> 100 MeV)	Significance[a]
3EG J0239+2815[b]	158.21°	-28.80°	5.1 ± 1.8	4.5 σ
3EG J0433+2908	170.48	-12.58	22.9 ± 3.6	13
3EG J0459+3352[a]	176.30	-5.38	3.8 ± 2.2	4.1
Unk.	179.3	-23.7	17.2 ± 3.5	7.8

[a] Near edge of region analyzed; flux underestimated.
[b] In Phase 1–5 data set.

Table 2 – Model Parameters by Energy Range

Energy Range (MeV)	A (10^{-26} s^{-1} sr^{-1})	B (10^{-26} s^{-1} sr^{-1} deg^{-1})	C (10^{-6} cm^{-2} s^{-1} sr^{-1} (K km s^{-1})$^{-1}$)	D (10^{-6} cm^{-2} s^{-1} sr^{-1})	X^a (10^{20} cm^{-2} (K km s^{-1})$^{-1}$)
100–10,000	2.02 ± 0.14	-0.052 ± 0.014	4.33 ± 0.25	6.3 ± 2.1	1.08 ± 0.10
300–10,000	0.82 ± 0.07	-0.030 ± 0.006	1.72 ± 0.11	< 1.1	1.06 ± 0.16
30–100	2.79 ± 0.38	-0.14 ± 0.03	<4.0	<22	
100–150	0.41 ± 0.06	-0.017 ± 0.006	0.66 ± 0.15	< 1.2	0.82 ± 0.22
150–300	0.50 ± 0.06	-0.012 ± 0.005	1.32 ± 0.11	< 2.1	1.34 ± 0.19
300–500	0.25 ± 0.03	-0.008 ± 0.003	0.46 ± 0.06	<0.3	0.93 ± 0.16
500–1000	0.17 ± 0.03	-0.006 ± 0.002	0.43 ± 0.05	<0.1	1.30 ± 0.27
1000–10,000	0.09 ± 0.02	<–0.003	0.33 ± 0.03	<0.2	1.52 ± 0.44

[a] Calculated including the propagation of the uncertainties in A and C, i.e., $X = C2\Delta[1 + (\sigma_A/A)^2]$ and $\sigma_X = \sigma_C/2\Delta[1 + (B\sigma_C/A\sigma_B)^2]^{-1/2}$.

4. Results

4.1. Point sources

The results of the search for point sources are shown in **Figure 3**, a composite map of likelihood test statistic. Maps for five energy ranges (100–150, 150–300, 300–500, 500-1000, and 1000-10,000 MeV) were examined to increase the sensitivity of the analysis. The contours are in units of source significance. Crosses indicate the positions of sources in the 3EG catalog (Hartman et al. 1999). Several of them are not detected in this analysis, most likely because they are variable and best detected in maps for individual viewing periods. In the present analysis, we include four point sources, with positions indicated with triangles (and tabulated in **Table 1**). The arc delineates the 10° radius around the Crab that was not included in the analysis.

The source near (179.3°, -23.7°), which is detected with 7.8 σ significance, may correspond to one or both of the unidentified sources 3EG J0423+1707 and 3EG J0426+1333. Both are catalogued as being detected in the Phase 1–4 composite dataset, although with complex source location contours. The intensified emission model used for the 3EG catalog appears to have a defect along the line l = 180° and the two sources may be artifacts. We do not investigate possible counterparts here, but note that MRC 0418+148 (179.80°, -24.08), a flat-spectrum radio source with flux 0.38 Jy at 4.85 GHz (Gregory & Condon 1991), lies just outside the 95% confidence contour (**Fig. 4**).

Figure 5 compares the gamma-ray intensity observed by EGRET with the maximum likelihood model (including the point sources of Table 1) for the representative energy range 10-0-10,000 MeV. (Again, the arc delineates the 10° region around the Crab that was not included in the analysis.) The residual (observed minus model) intensity map indicates no large-scale deviations. The brightest peak in the residual map, near (163°, -11°), is likely associated with 3EG J0416+3650, which was only marginally significant in this composite dataset and not included in our model; see **Fig. 3**. The maps in **Figure 5** were smoothed with a gaussian of FWHM 1.5° to reduce statistical fluctuations. Positions of point sources in the model (**Table 1**) are indicated with crosses.

The model (Eq. 2) was fit to the EGRET data for several energy ranges to derive the energy dependence of the gamma-ray emissivities (**Table 2**). We do not investigate the variations of the gradient term (B) here; the general decrease of emissivity with increasing latitude that the negative values found here imply is consistent with a decreasing cosmic-ray density across the outer Galaxy.

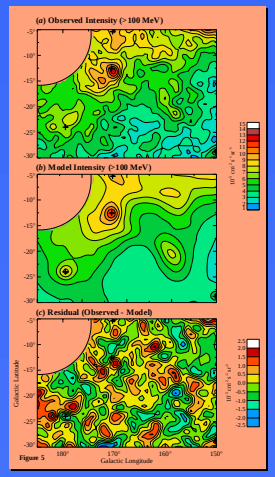

Figure 5

4.2. Molecular Mass Calibration

The value of X found here, (1.06 ± 0.16) × 10^{20} cm^2 (K km s^{-1})$^{-1}$ for energies above 100 MeV, is consistent with the values for other local clouds studied with EGRET (**Table 3**). Variations between the values in the table are consistent with an expected positive gradient of X toward the outer Galaxy (owing to generally decreasing metallicity and temperatures of interstellar gas with increasing Galactocentric distance).

The residual map in **Figure 5c** shows no evidence for variation of X within or between the Taurus and Perseus clouds, although the statistical uncertainties are high.

Table 3 – Local Emissivities and X-Ratios

Name	Longitude Range	Galactocentric Dist. (kpc)	X^a	Emissivity[b] (> 100 MeV)	(>300 MeV)
Ophiuchus (Hunter et al. 1994)	356–15°	8.4	1.1 ± 0.2	2.4 ± 0.2	1.0 ± 0.15
Cepheus (Digel et al. 1996)	100–130°	8.7	0.92 ± 0.14	1.84 ± 0.10	0.89 ± 0.06
Orion (Digel et al. 1999)	195–220°	8.9	1.35 ± 0.15	1.65 ± 0.11	0.71 ± 0.10
Monoceros (Digel et al. 2001)	210°–250°	9.2	1.64 ± 0.31	1.88 ± 0.17	0.88 ± 0.07
Taurus/Perseus (this work)	150–185°	8.6	1.08 ± 0.16	2.02 ± 0.14	0.82 ± 0.07

[a] Units: 10^{20} cm^2 (K km s^{-1})$^{-1}$
[b] Units: 10^{-26} s^{-1} sr^{-1}

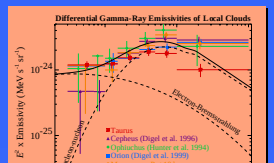

Figure 6

4.3. Gamma-ray emissivity

The differential gamma-ray emissivity in Taurus/Perseus is compared with other local cloud complexes in **Figure 6**. The only significant difference between Taurus/Perseus and the other clouds is at high energies; the well-known 'GeV excess' (Hunter et al. 1997) is not evident in Taurus. (The dashed lines show the predicted bremsstrahlung and pion-decay contributions to the emissivity based on spectra of cosmic-ray electrons and protons measured within the solar system; see Hunter et al. 1997). The origin of the GeV excess remains uncertain. On large angular scales, Strong, Moskalenko, & Reimer (2000) can explain the excess in terms of a harder spectrum of cosmic-ray electrons and a slightly modified spectrum of protons (their 'HEMN' model). In this model, most of the GeV excess is in fact inverse Compton emission.

We do not have enough evidence based on the analyses of local clouds to conclude that the excess is correlated with the interstellar gas, which would argue against an inverse Compton interpretation. In fact, the absence of a GeV excess in the Taurus/Perseus emissivity may be an artifact of our analysis, stemming from the inclusion of the emissivity gradient with latitude described above. The gradient term may partially compensate for the inverse Compton emission. Indeed, it may also subsume the extragalactic isotropic emission, which is detected in the present analysis only below 300 MeV, and with a lower than expected intensity (parameter D in **Table 2**).

The variations of integral emissivity among local clouds studied with EGRET are illustrated in the schematic overhead views shown in **Figure 7**. The emissivity above 300 MeV is due to cosmic-ray protons with GeV energies (see **Fig. 6**), and no significant variation between the local clouds is seen. The emissivity above 100 MeV has a much more significant contribution from cosmic-ray electrons, and for this energy range, significant variations are suggested in **Figure 7a**. Pohl & Esposito (1998) argue that density variations of cosmic-ray electrons are expected on even 100 pc scales owing to their rapid rate of energy loss.

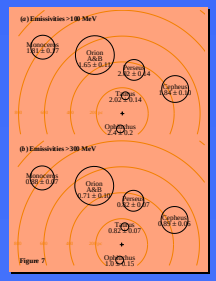

Figure 7

5. Conclusions

The interstellar emission observed by EGRET in the Taurus/Perseus region can be well described by a simple model that accounts for the distribution of the interstellar gas across the outer Galaxy by allowing the gamma-ray emissivity for the total column density of gas to have a linear gradient with latitude within 15° of the plane.

Within the region analyzed, four point sources were detected. One of them is not in the 3EG catalog and may be an improved explanation for two closely separated unidentified sources in the catalog.

The molecular mass calibrating ratio X is consistent with that found for other local clouds, and no significant variation of X within or between the clouds in Taurus and Perseus were found (although the variations cannot be tightly constrained, owing to the limited gamma-ray statistics).

The integral emissivity above 300 MeV, which primarily traces the density of GeV cosmic-ray protons, does not vary significantly among any of the local clouds studied with EGRET. The emissivity above 100 MeV has significant variations, which can be understood in terms of expected density variations of cosmic-ray electrons on even 100 pc scales.

References

Dame, T. M., Hartmann, Dap, & Thaddeus, P. 2001, ApJ, 547, 792

Dickman, R. L., 1978 ApJS, 37, 407

Digel, S. W., et al. 1996, ApJ, 464, 609

Digel, S. W., et al. 1999, ApJ, 520, 196

Digel, S. W., et al. 2001, ApJ, in press

Gregory, P. C., & Condon, J. J. 1978, ApJS, 75, 1011

Hartman, R. C., et al. 1999, ApJS, 123, 79

Hartmann, Dap, & Burton, W. B. 1997, Atlas of Galactic Neutral Hydrogen, Cambridge University Press

Hunter, S. D., Digel, S. W., de Geus, E. J., & Kanbach G. 1994, ApJ, 436, 216

Hunter, S. D., et al. 1997, ApJ, 481, 205

Lebrun, F., et al. 1983, A&A, 274, 231

Mattox, J. R., et al. 1996, ApJ, 461, 396

Pohl, M. & Esposito, J. A. 1998, ApJ, 507, 327

Strong, A. W., Moskalenko, I. V., & Reimer, O. 2000, ApJ, 537, 763